REPORT DOCUMENTATION PAGE

Form Approved
OMB No. 0704-0188

1. AGENCY USE ONLY *(Leave blank)*	2. REPORT DATE	3. REPORT TYPE AND DATES COVERED
	15.Dec.03	MAJOR REPORT

4. TITLE AND SUBTITLE
"THERMAL CONDUCTIVITY EVOLUTION DURING INITIAL STATE SINTERING"

5. FUNDING NUMBERS

6. AUTHOR(S)
MAJ SCHLAEFER CONSTANCE E

7. PERFORMING ORGANIZATION NAME(S) AND ADDRESS(ES)
PENNSYLVANIA STATE UNIVERSITY

8. PERFORMING ORGANIZATION REPORT NUMBER
CI02-1315

9. SPONSORING/MONITORING AGENCY NAME(S) AND ADDRESS(ES)
THE DEPARTMENT OF THE AIR FORCE
AFIT/CIA, BLDG 125
2950 P STREET
WPAFB OH 45433

10. SPONSORING/MONITORING AGENCY REPORT NUMBER

11. SUPPLEMENTARY NOTES

12a. DISTRIBUTION AVAILABILITY STATEMENT
Unlimited distribution
In Accordance With AFI 35-205/AFIT Sup 1

DISTRIBUTION STATEMENT A
Approved for Public Release
Distribution Unlimited

12b. DISTRIBUTION CODE

13. ABSTRACT *(Maximum 200 words)*

20040105 011

14. SUBJECT TERMS

15. NUMBER OF PAGES
9

16. PRICE CODE

17. SECURITY CLASSIFICATION OF REPORT	18. SECURITY CLASSIFICATION OF THIS PAGE	19. SECURITY CLASSIFICATION OF ABSTRACT	20. LIMITATION OF ABSTRACT

THERMAL CONDUCTIVITY EVOLUTION DURING INTIAL STAGE SINTERING

Constance E. Schlaefer
Randall M. German
Center for Innovative Sintered Products
The Pennsylvania State University
University Park PA 16802-6809 USA

ABSTRACT

The effective thermal conductivity of injection-molded material is useful as a means of monitoring initial stage sintering. Data obtained via laser flash analysis are inputs for a model relating thermal conductivity to strength. Multiple measurements can be made during a single sintering cycle, detailing the growth of interparticle bonds and onset of handling strength.

INTRODUCTION

The onset of sintering represents a transition from individual particles to a cohesive network of solid material. This transition is reflected in the physical and mechanical properties of the material, so the measurement of these properties may be used to infer the degree of sintering. Much work has been done in the study of properties at higher density, resulting in many physical and mechanical models based on porosity. However, the inherent difficulty of measuring properties of a powder as it is beginning to bond has limited experimental investigation of this critical transition point in the sintering process. This difficulty, due to the very fragile nature of the material at the onset of sintering, defines the motivation and the proposed methods of this research. This work investigates the hypothesis that sintering evolution can be observed through the observation of thermal properties, and translated to a prediction of mechanical strength. Laser flash analysis, which is a non-contact technique for directly measuring thermal diffusivity in a material, presents such a means for measuring the *in situ* evolution of thermal properties.

EXPERIMENTAL PROCEDURES

Nickel was chosen as a baseline system due to its stable nature—no solid phase changes, and resistance to persistent oxidation. The candidate powder, Novamet 4SP-10, is a carbonyl nickel powder with relatively low surface roughness (versus the spiky surface normally associated with carbonyl nickel) and spherical shape. The powder is screened for a narrow particle-size distribution--80% of the powder is between 4 and 11 micrometers, with a median particle size of 7 micrometers.

Samples were fabricated using a polymer-wax binder system. The nickel powder was combined in a 58 volume % mixture with the binder powders. The binder mixture consisted of 50 weight % paraffin wax (BP 7355 Paraffin Wax), 40 weight % polypropylene (PolyVisions ProFlow 3000), and 10 % linear low-density polyethylene (DuPont Fusabond MB-2260D). Transverse rupture bars (32 mm x 12.79 mm x 3.25 mm) were molded on a 30-ton reciprocating screw injection-molding machine (model: 270V; supplier: ARBURG, Inc., Newington, CT). Disks were cut from the bars using a heated circular stamp, 12.79 mm in diameter. The samples were solvent- debound in a warm heptane bath (60°C for 120 minutes) to remove the paraffin wax.

Batches of samples were prepared to assess the evolution of thermal conductivity and bend strength at increments along the thermal debind cycle. Each sample set was composed of two disks and three TRBs. Sets were thermally debound at 2°C/min, with a 2-hour hold at 425°C, as shown in Figure 1. Each mark on the graph indicates a set of samples which were debound to that point in the cycle, held at constant temperature for 15 minutes while the furnace was purged of hydrogen, then removed from the sintering furnace and air-cooled. A second set of samples was thermally debound along the same profile through the 2-hour hold, then heated at 10°C/min to 500, 600, or 700°C.

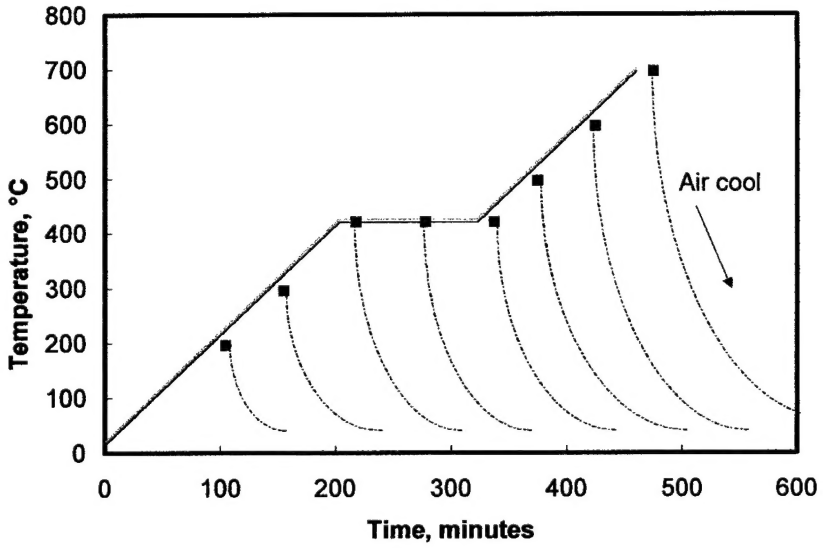

Figure 1: Time-temperature profile for thermal debinding of PIM transverse rupture bars and thermal diffusivity disks. Samples were heated at 2°C/min, with a 2-hour hold at 425°C in flowing hydrogen. Sets of bars and disks were removed at the increments shown, and cooled in air.

Transverse rupture tests were performed on a Sintech 20/D electromechanical load frame with an MTS 4450 N (1000 lb) load cell in standard 3-point bend configuration. Test execution and data management were controlled using Testworks software. Crosshead movement was displacement-controlled at a constant rate of 2 mm/minute. Data acquisition was performed by a digital controller at 1000 Hz.

Thermal diffusivity measurements were made using the laser flash technique on an Anter Flashline™ 5000 system. Two 12 mm presintered samples were supported side by side in an alumina holder, encased in a Super Kanthal™ radiant furnace, with a flowing nitrogen atmosphere. Measurements were made at

100°C. During each measurement, an Nd/glass laser projected a beam through a quartz window into the furnace, illuminating the top face of the 12 mm sample disk. An In/Sb infrared sensor viewed the bottom face through a sapphire window and mirror relay, recording the equilibrium temperature, and the subsequent temperature rise at a rate of 15 kHz. Three data points were taken on each sample. Thermal conductivity was calculated using Equation 1:

$$\kappa = \alpha C_P \rho_s \qquad (1)$$

where κ is thermal conductivity (W/m·K), α is the measured thermal diffusivity (m^2/s), C_p is the specific heat of wrought nickel at the test temperature (J/kg·K), and ρ_s is the sintered density of the porous material (kg/m^3).

RESULTS AND DISCUSSION

Room temperature transverse rupture strength results for injection-molded bars are shown in Figure 2. The green strength for the solvent-debound PIM material was 5.3 MPa, rising to 23 MPa at 200°C, and then dropping to 0.5 MPa at 425°C. Only after two hours at 425°C is there an increase in strength from 0.5 to 1.0 MPa. At higher temperatures, strength increases dramatically, reaching 98 MPa at 700°C. Shown with the strength measurements are the corresponding fractional densities (measured dimensionally) with increasing peak sintering temperature. An increase in fractional density from 58 to 59 % occurs between room temperature and 200°C, corresponding with the increase in transverse rupture strength.

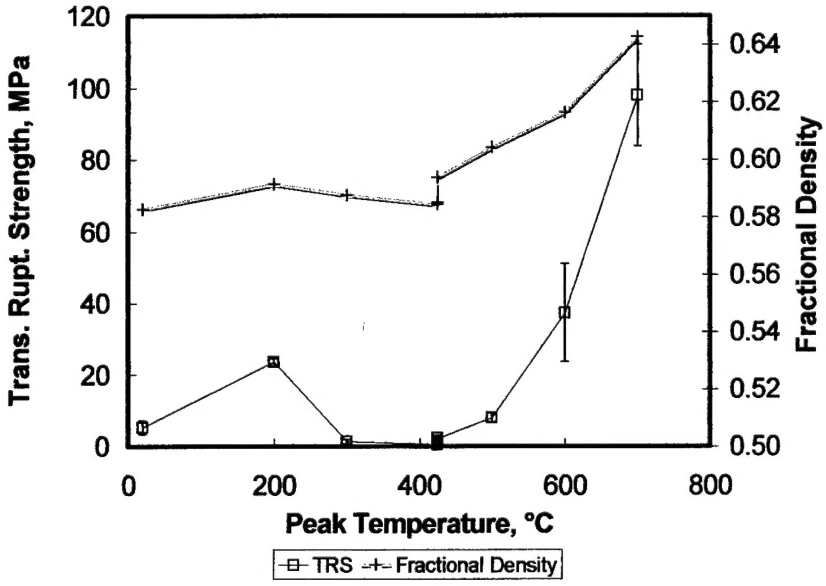

Figure 2: Room temperature transverse rupture strength and density of PIM samples versus peak sintering temperature. Samples were heated at 2°C/min in flowing hydrogen to 425°C, held for 2 hours, and heated at 2°C/min to 700°C.

Although these measurements were taken at room temperature, the effect of binder melting and flowing during previous heating alters the subsequent behavior. Since the polymer melts by 140°C, the sample

treated at 200°C has already experienced this phase change. The polymer flowed to the interparticle contact points to create pendular bonds, drawing the particles together and increasing the overall strength and density of the specimen.

Normalized thermal conductivity versus peak sintering temperature results are shown for the 2°C/min heating rate samples in Figure 3. *In situ* measurements of raw powder with no binder are shown for comparison. Thermal conductivity of the injection-molded material remained essentially constant at 3-4 % that of solid nickel, up to the hold temperature of 425°C. Only after two hours at the hold temperature did the thermal conductivity increase to 7 %. Following the hold, a linearly increasing trend between thermal conductivity and temperature was observed.

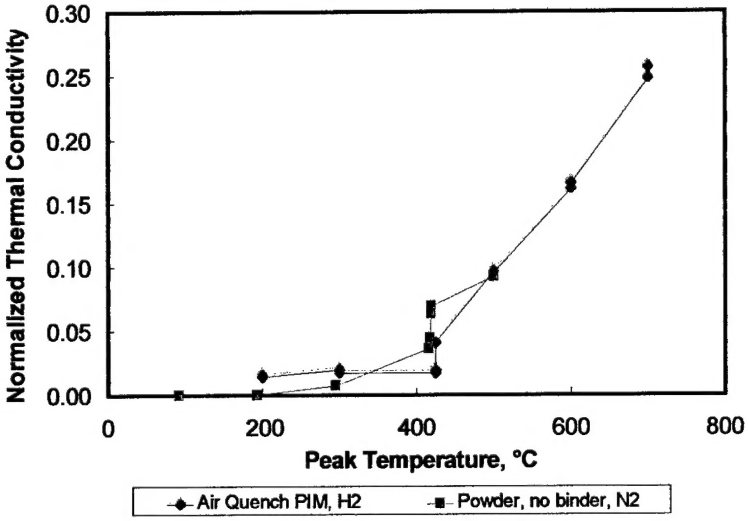

Figure 3: Measured thermal conductivity versus peak temperature for PIM material and raw powder. PIM material measured at 100°C, powder measured *in situ*. Both sets of measurements are normalized by wrought values at the measurement temperature.

The constant thermal conductivity through the one-hour hold at 425°C is consistent with binder presence in the material. Measured conductivity of the debinding material was significantly higher at this temperature than that of the raw powder. This difference implies that the solid binder material still present at the interparticle contacts increases the overall effective conductivity versus the same metal powder with only gas in the pores. Although the polymer has a relatively low thermal conductivity compared to metal, it is still much more conductive than gas (approximately 1 W/m/K versus 0.02 W/m/K). The implication is that even the smallest bit of remaining polymer at the interparticle contact strongly influences the overall conductivity of the debinding material. As early as 300°C, the raw powder begins to show increases in thermal conductivity, indicating the initiation of sinter bonds, even in a non-reducing atmosphere. During the hold, the thermal conductivity of the raw powder evolved more rapidly than that of the PIM material, implying that the presence of the binder impedes the initial growth of the neck below the thermal debind temperature. This is consistent with a reduced level of surface diffusion in the presence of the polymer layer.

The relationship between strength and thermal conductivity was examined using a linear plot of the logarithm of normalized TRS versus the logarithm of the normalized thermal conductivity. The slope of the linear plot, shown in Figure 4, was determined to describe the relationship between the two properties. The slope of approximately two strongly supports a second order relationship between strength and thermal conductivity during initial stage sintering, not the first order (linear) relationship initially expected. Existing strength models show a squared dependence on interparticle neck diameter. Xu[1] and German[2] proposed a strength model incorporating dependence on neck size as shown in Equation 2:

$$\sigma_{ult} = \frac{\sigma_o V_s N_c}{K\pi}\left[\frac{X}{D}\right]^2 \qquad (2)$$

where K is a stress concentration factor related to neck curvature, V_s is the fractional density (measured density normalized with respect to theoretical density), N_c is the coordination number, and σ_o is the wrought strength (MPa) as a function of temperature. In considering this relation, K may be described in terms of neck size ratio, as shown in Equation 3:

$$K = \frac{1}{2}\left[\frac{X}{D}\right]^{-2} \qquad (3)$$

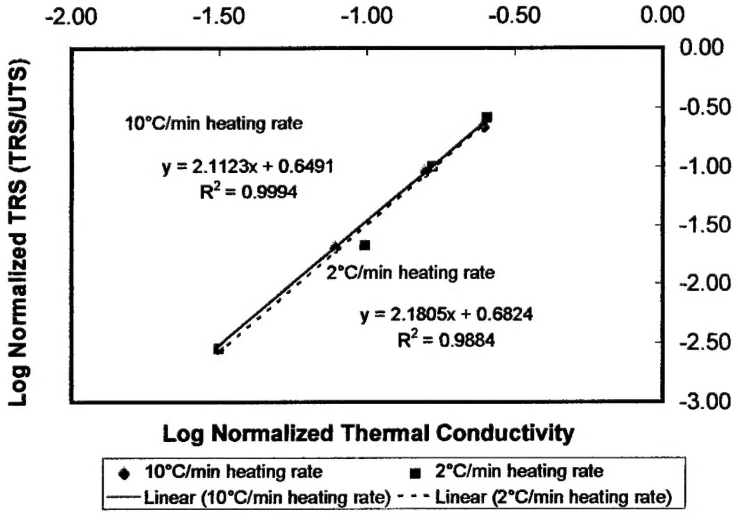

Figure 4: Strength normalized by wrought ultimate tensile strength versus thermal conductivity normalized by wrought thermal conductivity for 10°C/min and 2°C/min samples. Samples were heated in flowing hydrogen at the prescribed heating rate, removed from the furnace and air-cooled. Strength was tested at room temperature, conductivity tested at 100°C. Results were normalized by wrought values at the test temperature.

Thermal conductivity, commonly modeled as a circuit of thermal resistance elements, was also expected to vary with the neck area, a squared function of the neck diameter. A description of a single cylindrical thermal element in the circuit is shown in Equation 4:

$$\kappa_{eff} = \frac{\kappa A}{L} = \frac{\kappa \left(\frac{\pi}{4}\right)(X)^2}{\left(\frac{D}{2}\right)} \qquad (4)$$

where κ is the conductivity of the bulk material. A is the contact area between elements of the model, which models the area of the interparticle neck, and L is the length of the resistance element. X is the diameter of the circular contact area, and D is the particle diameter. Equation 4 was modified to normalize the neck diameter, as shown in Equation 5, creating a common neck size ratio term, X/D, between the strength and conductivity models.

$$\kappa_{eff} = \frac{\kappa A}{L} = \frac{\kappa \left(\frac{\pi}{4}\right)\left(\frac{X}{D}\right)^2 D^2}{\left(\frac{D}{2}\right)} \qquad (5)$$

Neck diameter (X) was measured via scanning electron microscope (SEM) to investigate actual neck size and correspondence to these models. Fracture faces were examined for ruptured interparticle bonds, shown as light spots on the particle surface in Figure 5. Measured diameters were normalized by the median particle diameter of a population-based distribution. A comparison of strength versus neck size indicated that Xu and German's strength model underestimated strength for this system. Observed plasticity at the ruptured necks prompted the incorporation of true stress, versus engineering stress, as a parameter in Equation 2, yielding the modified version for ductile material shown in Equation 6.[3]

$$\sigma_{ult} = \frac{\sigma_{eng}\left(1+\varepsilon_{eng}\right)V_s N_c}{K\pi}\left[\frac{X}{D}\right]^2 \qquad (6)$$

where σ_{eng} is the wrought ultimate tensile strength at the test temperature, and ε_{eng} is the percent elongation at failure at the test temperature.

Comparison of the thermal circuit model with measured results showed that use of the squared neck size significantly underestimated thermal conductivity. Instead, a linear relationship between neck size and thermal conductivity was confirmed, as shown in Figure 6.

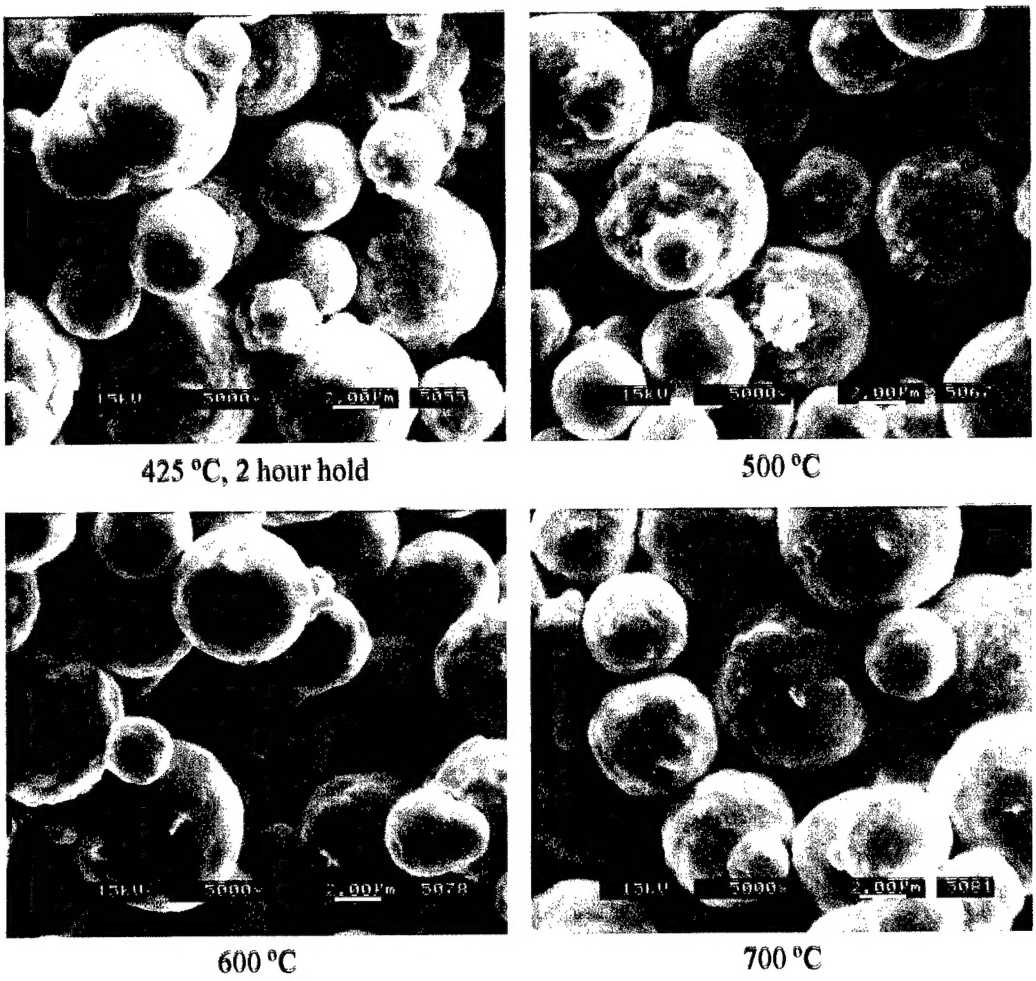

Figure 5: SEM images of fracture surfaces for PIM material at increasing sintering temperatures. Samples fractured by three-point bend testing at room temperature. Light spots indicate fractured interparticle bonds.

The existing strength model and the linear model for thermal conductivity for this system can be combined based on their mutual dependence on neck size. This integrated relationship is shown in Equation 7:

$$\sigma_{ult} = \sigma_{eng}\left(1+\varepsilon_{eng}\right)\frac{V_s N_c}{K\pi}\left[\left(\frac{\kappa_{eff}}{\kappa_o}-\gamma\right)\frac{1}{\chi}\right]^2 \qquad (7)$$

where γ and χ are system dependent parameters equal to 0.56 and 0.021 respectively for this system. This relation can be used to predict transverse rupture strength by applying a factor of 1.6 to the ultimate tensile strength, σ_{ult}, predicted in Equation 6.[2] Although currently system dependent, once the thermal conductivity relationship to neck size is profiled, strength can be predicted at any point, either *in situ* or at

room temperature, if handbook values for wrought strength, percent elongation, and thermal conductivity at the temperature of interest are known.

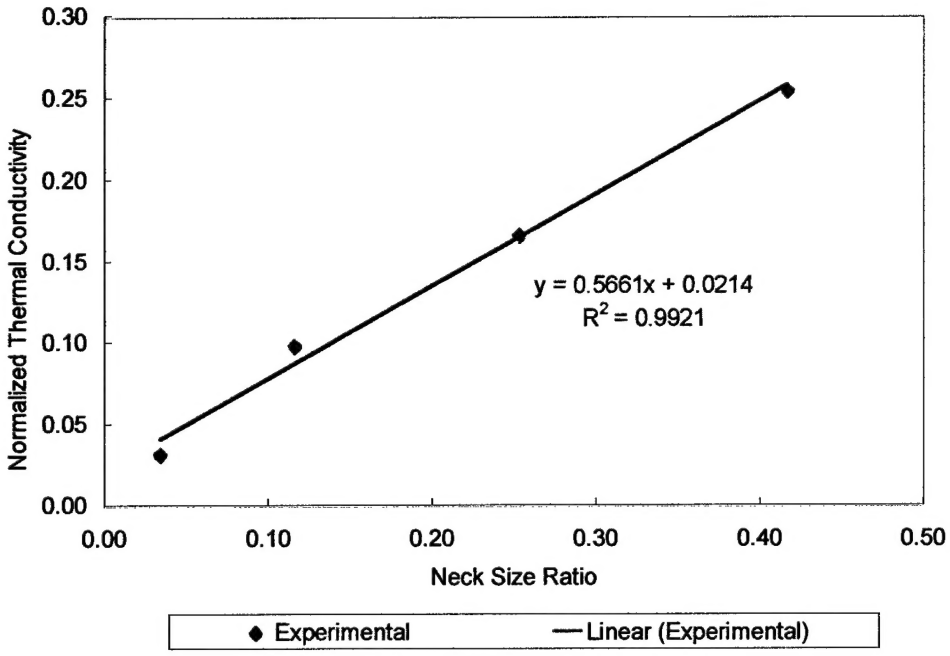

Figure 6. Thermal conductivity versus neck size ratio (X/D) for 10°C/min samples. Neck size was measured via SEM by observing ruptured bond sites on a fracture face. Neck size was normalized by median particle size based on a population distribution.

CONCLUSIONS

A technique to assess thermal conductivity of powder metallurgy materials has been developed and modeled. Thermal conductivity during early stage sintering has been shown to be a linear function of neck size, versus a squared function as expected. Profiling a system for such a model must include an additional assessment of neck size, via SEM, as demonstrated in this work, or by some alternate method. Once an initial profile is established, neck size may be extracted from *in situ* laser flash measurements under any sintering conditions of interest.

A clear relationship between the evolution of thermal conductivity and mechanical strength has been demonstrated. Both properties are functions of neck size; therefore if neck size can be inferred from thermal conductivity evaluation, mechanical strength can be assessed. Laser flash analysis, as a non-contact measurement, overcomes the difficulties of measuring strength mechanically in a fragile material, providing the capability of a non-destructive means of assessing the onset of handling strength.

ACKNOWLEDGEMENTS

The authors gratefully acknowledge tuition support from the United States Air Force, research funding from the Brush Chair for Materials, and a university grant from Anter Corporation as partial funding for the Flashline™ 5000 thermal diffusivity analysis system.

The views expressed in this article are those of the author and do not reflect the official policy or position of the United States Air Force, Department of Defense, or the U.S. Government.

REFERENCES

[1] X. Xu, "Densification and Strength Evolution in Solid-State Sintering. Part II. Strength Model," *Journal of Materials Science*, 2002, vol.. 37, pp. 117-126.

[2] R. M. German, "Manipulation of Strength During Sintering as a Basis for Obtaining Rapid Densification without Distortion," *Materials Transactions*, 2001, vol. 42, no. 7, pp. 1400-1410.

[3] R. W. Hertzberg, *Deformation and Fracture Mechanics of Engineering Materials*, 3rd edition, John Wiley and Sons, New York, NY, 1989, p. 4.